Analytica Chimica Acta 651 (2009) 36–41

Contents lists available at ScienceDirect

Analytica Chimica Acta

journal homepage: www.elsevier.com/locate/aca

High dielectric constant PrY_xO_y sensing films electrolyte-insulator-semiconductor pH-sensor for the detection of urea

Min-Hsien Wu [a], Cheng-Da Lee [b], Tung-Ming Pan [b,*]

[a] Graduate Institute of Biochemical and Biomedical Engineering, Chang Gung University, Taoyuan 333, Taiwan, ROC
[b] Department of Electronics Engineering, Chang Gung University, Taoyuan 333, Taiwan, ROC

ARTICLE INFO

Article history:
Received 14 July 2009
Received in revised form 5 August 2009
Accepted 7 August 2009
Available online 18 August 2009

Keywords:
Electrolyte-insulator-semiconductor
PrY_xO_y
pH sensitivity
Urea

ABSTRACT

In this paper, we describe the structural and sensing properties of high-*k* PrY_xO_y sensing films deposited on Si substrates through reactive co-sputtering. Secondary ion mass spectrometry and atomic force microscopy were employed to analyze the compositional and morphological features of these films after annealing at various temperatures. The electrolyte-insulator-semiconductor (EIS) device incorporating a PrY_xO_y sensing membrane that had been annealed at 800 °C exhibited good sensing characteristics, including a high sensitivity (59.07 mV pH^{-1} in solutions from pH 2 to 12), a low hysteresis voltage (2.4 mV in the pH loop $7 \rightarrow 4 \rightarrow 7 \rightarrow 10 \rightarrow 7$), and a small drift rate (0.62 mV h^{-1} in the buffer solution at pH 7). The PrY_xO_y EIS device also showed a high selective response towards H^+. This improvement can be attributed to the small number of crystal defects and the large surface roughness. In addition, the enzymatic EIS-based urea biosensor incorporating a high-*k* PrY_xO_y sensing film annealed at 800 °C allowed the potentiometric analysis of urea, at concentrations ranging from 1 to 16 mM, with a sensitivity of 9.59 mV mM^{-1}.

1. Introduction

The first material used as a pH-sensitive membrane for the ion-sensitive field-effect transistor (ISFET) was SiO_2 dielectric, introduced by Bergveld [1] in 1970. However, there were still disadvantages in the ISFET sensing structure that required to be improved, such as the poor isolation between the devices and the chemical solutions, and the sensitivity optical effects. The ion-selective electrode was deposited directly onto the field-effect transistor (FET) to form the ISFET device. Conventional gate electrodes are usually based on a pH selective glass membrane. Many metal oxides, instead of a noble metal, are employed to fabricate the pH electrode material. Fog and Buck [2] reported that a large number of metal oxides including PtO_2, IrO_2, RuO_2, OsO_2, Ta_2O_5, and TiO_2 were produced from metal powders or oxidized metal. The pH value is an important parameter for different application fields including clinical diagnosis, industrial wastewater measurement, and environmental pollution monitoring.

Since Caras and Janata [3] developed a penicillin-sensitive biosensor based on pH-ISFET, enzyme ISFET (EnFET) devices have attracted much attention for medical, pharmaceutical, and biotechnical applications because they have the advantages of rapid response, low cost, compact size, high reliability, low output impedance, and ease of fabrication. EnFET biosensors are usually constructed by immobilizing an enzyme onto the gate dielectric of an ISFET. The most critical point of the EnFET configuration is the attachment of the enzyme or the enzyme-containing layer to the underlying inorganic gate insulator material of the FET. Generally, the working principle of an EnFET can be explained in the following way: during the enzymatic reaction of the enzyme with its substrate, either products are generated or reactants are consumed, and this concentration change can be detected by the underlying ISFET. Consequently, a corresponding change of the ISFET signal can be correlated with the original analyte concentration.

The sensing characteristics of EnFET biosensor are strongly dependent on performance of the ISFET based pH sensing mechanism. Silicon nitride (Si_3N_4) sensing membrane is the most popular material of choice for pH-ISFET mainly due to the ease of fabrication, high compatibility for complementary metal-oxide-semiconductor (CMOS) integration [4]. However, pH-ISFET devices with a Si_3N_4 sensing membrane show unstable properties on threshold voltage arising from the conversion of silicon nitride film to a hydrated silicon dioxide (SiO_2) or an oxynitride layer during the contact with an aqueous solution [5]. In order to solve this issue, high dielectric constant (high-*k*) materials, including SnO_2, WO_3, ZrO_2, HfO_2, Y_2O_3, Pr_2O_3, and Gd_2O_3 [6–12] were recently proposed as a pH sensing membrane borrowing from their good sensing performance and highly thermal stability. A thin SiO_2 film was thermally grown on

* Corresponding author. Tel.: +886 3 211 8800x3349; fax: +886 3 211 8507.
E-mail address: tmpan@mail.cgu.edu.tw (T.-M. Pan).

0003-2670/$ – see front matter © 2009 Elsevier B.V. All rights reserved.
doi:10.1016/j.aca.2009.08.006

silicon substrate to interface the above high-*k* film and a silicon substrate. This was proved not only to form interface properties with small density but also to provide a fabrication scheme with low stress and good adhesion [13].

Besides those previously mentioned high-*k* materials, it has also reported recently that the rare-earth (RE) oxide films [14] are potential materials for gate insulation due to their reasonably high relative permittivity, good thermal stability, and large conduction band offset. However, many low permittivity RE films were reported [15]. The low permittivity is mainly attributed to the low density of amorphous La_2O_3 films or the moisture absorption which deteriorates the permittivity of La_2O_3 films because of the formation of the low permittivity lanthanum hydroxide [16]. In order to overcome this problem, a high permittivity $La_{1-x}Y_xO_y$ film was studied as an alternative gate insulator because Y_2O_3 film has a much stronger resistance to the moisture than the La_2O_3 film [17]. In this paper, we describe the physical properties and sensing characteristics of the high-*k* PrY_xO_y films deposited on a Si (1 0 0) substrate through reactive co-sputtering. We have used secondary ion mass spectrometry (SIMS) to monitor the chemical composition of the PrY_xO_y films and atomic force microscopy (AFM) to measure the surface morphology of the PrY_xO_y sensing films after annealing at various temperatures. Furthermore, we determined the effect that postdeposition annealing (PDA) treatment had on the sensing characteristics (pH sensitivity, hysteresis, drift, and selectivity) of these PrY_xO_y films. In addition, as a demonstration case for enzymatic EIS-based urea biosensor, urease-immobilized membrane was prepared by the entrapment of enzyme molecules in alginate hydrogel.

2. Experiment

2.1. Fabrication of EIS pH-sensor

High-*k* PrY_xO_y EIS devices were fabricated on 10 cm p-type Si (1 0 0) wafers having a resistivity of 5–10 Ω cm. Before the deposition of PrY_xO_y, the wafers were cleaned using a standard RCA process and followed by dipping into a dilute 1% HF solution to remove the chemical oxide layer. A PrY_xO_y film with thickness of about 21 nm was then deposited on Si substrate through the co-sputtering Pr and Y from a praseodymium target and a yttrium target under the argon-to-oxygen (Ar/O_2) ratio of 15/15. The wafers were subsequently annealed using a conventional rapid thermal annealing (RTA) system under ambient O_2 condition for 30 s at various temperatures (700, 800, and 900 °C). The back-side contact (a 400-nm-thick Al film) of the Si wafer was deposited using a thermal coater. The sensing membrane size was defined through photolithographic processing under a photosensitive epoxy (SU8-2005, MicroChem) that behaved as an anti-acid polymer. EIS devices were then fabricated on the Cu lines of a printed circuit board by using an Ag gel to form conductive lines. A handmade epoxy package was employed to encapsulate the EIS structure and the Cu line.

2.2. Evaluation of the structural properties and pH sensing performance

The composition of the PrY_xO_y sensing membranes annealed at different temperatures was investigated using SIMS. The surface morphologies of PrY_xO_y films were examined by AFM. On the other hand, the pH sensitivities of PrY_xO_y films were determined by measuring the capacitance–voltage (*C–V*) curves of the EIS structures. The *C–V* curves were measured using buffer solutions of various values of pH (Merck), an Ag/AgCl reference electrode, and a Hewlett–Packard 4284A LCR meter operated at an alternating current (ac) signal frequency of 100 Hz to maintain the electrochemical system at equilibrium. All setups were performed in a dark box to avoid interference from light and noise. To balance the surface reactions, all of the EIS samples were submerged in reversed-osmosis water for 12 h prior to performing the electrical measurements.

2.3. Urea biosensor

A urease (from Jack Beans, ~100 U mg^{-1}; unless otherwise stated, all chemicals were purchased from Sigma) solution prepared in phosphate-buffered saline (PBS) was thoroughly mixed with an alginate suspension to form a urease/alginate suspension having concentrations of 0.1 mg L^{-1} and 1.5% (w/v), respectively. The suspension was loaded onto a clean glass slide and then covered with another glass slide, leaving a 1-mm-thick spacer in between to define the thickness of the alginate thin layer. In the subsequent gelatinization process, the sandwich-like structure was submerged in 102 mM $CaCl_2$ for ~10 min. A thin urease-containing alginate gel was subsequently shaped according to the zone of the PrY_xO_y sensing membrane using a borer; it was then attached to the surface of the sensing membrane. Urea solutions having concentrations of 1, 2, 4, 8, and 16 mM were prepared from urea powder and PBS; the pH in each solution was measured using a commercial pH meter.

3. Results and discussion

3.1. Structural properties

Fig. 1 shows the SIMS depth profiles of PrY_xO_y film that has been annealed at 800 °C. The composition of the film annealed at 800 °C showed a PrY_xO_y compound with a Pr:Y:O ratio of approximation 2:1:5. It is found that a small amount of silicate layer ($PrSi_xO_y$) forms at the interface between the dielectric film and the Si substrate. For silicate formation in the film, the reaction progressed by diffusion of Si from the substrate to the dielectric layer [14].

Fig. 2 depicts the AFM surface images of the PrY_xO_y films annealed at different temperatures. The surface roughness of the PrY_xO_y films clearly increased upon increasing the RTA temperature. The PrY_xO_y film performed at 700 °C possessed a smooth surface (0.518 nm), whereas the one annealed at 900 °C showed a rough surface (2.632 nm). We suggest that this behavior is due to an increased self-diffusion of yttrium, praseodymium and oxygen during high-temperature annealing leading to the enhancement of the clustering of grains, thus increasing the surface roughness of the PrY_xO_y film [18].

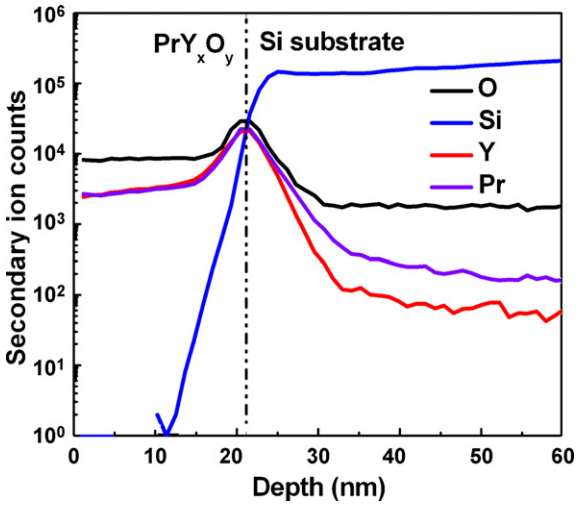

Fig. 1. SIMS profiles of a PrY_xO_y film after RTA at 800 °C.

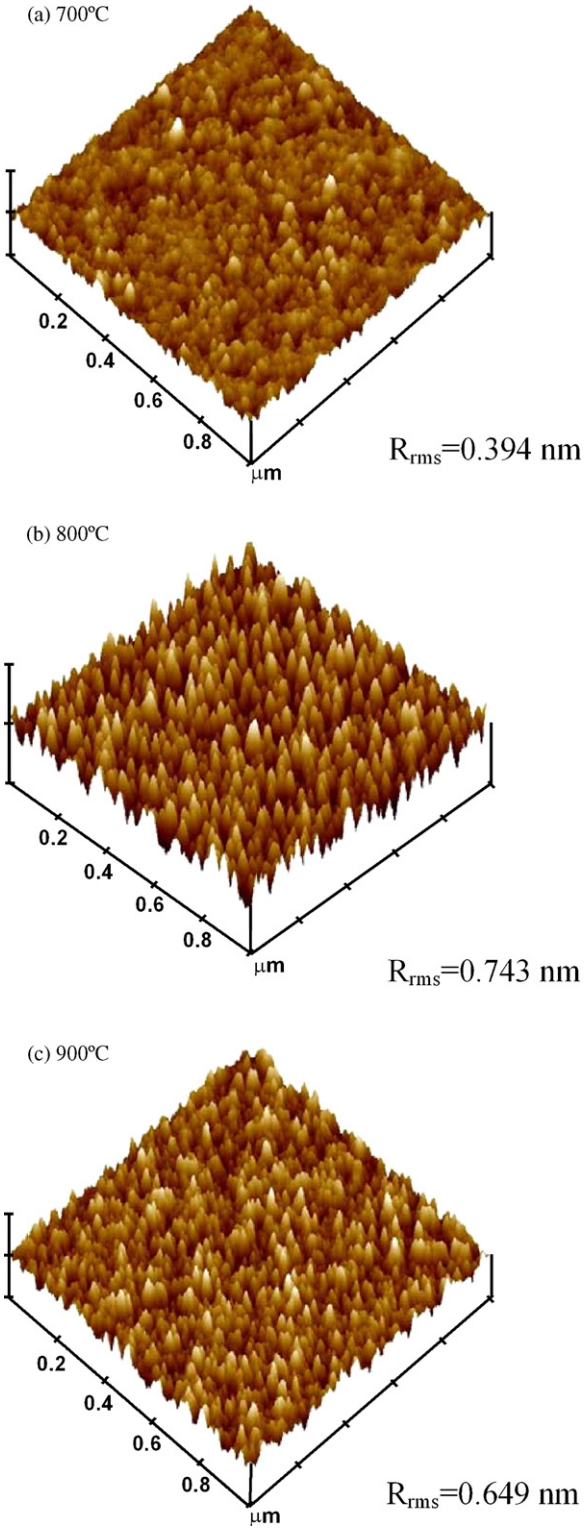

Fig. 2. AFM surface images of PrY_xO_y sensing films for: (a) 700 °C (b) 800 °C, and (c) 900 °C.

3.2. Sensing characteristics of pH–EIS sensor

The effect of the PDA temperature on the pH sensitivity of the PrY_xO_y sensing membrane can be understood by considering the site-binding model to describe the ionic absorption processes at the electrolyte/oxide interface [19]. The reference voltage depends on the surface potential (ψ), which relies on the acido-basic properties of the sensitive material and on the electrolyte pH. The value of ψ can be obtained from the Eq. (1):

$$\psi = 2.303\frac{kT}{q}\frac{\beta}{\beta+1}\left(\mathrm{pH}_{pzc} - \mathrm{pH}\right) \quad (1)$$

where k is Boltzmann's constant, T is the temperature of the system, q is the elementary charge, pH_{pzc} is the pH at the point of zero charge, and β is a parameter that indicates the chemical sensitivity of the gate oxide—it is dependent on the density of surface hydroxyl groups [20]. The pH_{pzc} of pH-ISFET is given by the Eq. (2):

$$\mathrm{pH}_{pzc} = -\log_{10}\left(\frac{K_a}{K_b}\right)^{0.5} \quad (2)$$

where K_a and K_b represent the equilibrium constants at acid and base point, respectively. Moreover, the β value is relevant to the chemical sensitivity of gate dielectric and is determined by the density of surface hydroxyl groups, which is given as the Eq. (3).

$$\beta = \frac{2q^2 N_s\sqrt{K_a K_b}}{kTC_{DL}} \quad (3)$$

where N_s is the total number of surface site per unit area and C_{DL} is the double layer capacitance derived from the Gouy–Chapman–Stern model [21]. Based on the above equations, it can be supposed that the higher N_s (or the higher β) accordingly contributes to a higher sensitivity and also the more linear response of pH detection [11]. Based on the value reported in the literature [21], we assume that the double layer capacitance is 20 μF cm^{-2} for PrY_xO_y EIS device performed at different RTA temperatures. The values of N_s, K_a, and K_b can be calculated from the pH_{pzc} and β, according to Eqs. (2) and (3). The obtained N_s, K_a, and K_b values are then related to the sensing performance of the PrY_xO_y EIS devices annealed at different PDA temperatures. The results are summarized in Table 1. These values are in good agreement with the literature reported in Ref. [22].

Table 1
The pH_{pzc}, β, N_s, K_a, and K_b of high-k PrY_xO_y sensing membranes annealed at different temperatures.

RTA temperature (°C)	pH_{pzc}	β	N_s (cm^{-2})	K_a	K_b
700	5.11	35.82	5.17×10^{14}	$10^{-6.1}$	$10^{4.2}$
800	9.07	129.41	5.65×10^{14}	$10^{-9.5}$	$10^{8.6}$
900	7.89	83.19	5.36×10^{14}	$10^{-8.5}$	$10^{7.3}$

In pH–EIS sensing characteristics, the variation in the pH of the solution led to a shift in the flatband voltage of the C–V curves. This result is mainly due to the ionization of the surface hydroxyl groups by either hydrogen ions or hydroxyl ions. To evaluate the sensing performance of the PrY_xO_y membrane annealed at different temperatures, we recorded a set of C–V curves at the pH ranging from pH 2 to 12. Fig. 3 demonstrates the pH-dependence of the reference voltage (the voltage required to achieve a normalized capacitance of 0.5) of a PrY_xO_y EIS device that had been subjected to PDA at 800 °C. During a cycle from pH 2 to 12, the pH sensitivity of this PrY_xO_y film was 59.07 mV pH^{-1}. The inset to Fig. 3 shows the pH-dependence of one group of C–V curves for the EIS structure incorporating a PrY_xO_y sensing film annealed at 800 °C. These normalized C–V curves were shifted as a result of the variation in the number of hydrogen ion on the sensing membrane. It is found that a PrY_xO_y EIS device annealed at 800 °C exhibited a better sensitivity than those of the devices performed at the other RTA temperatures, as shown in Table 2. This result could be attributed to the higher surface roughness of PrY_xO_y sensing membrane annealed at 800 °C as observed in the previous AFM analysis. With the higher surface roughness, the N_s will increase accordingly, which therefore contributes to higher detection sensitivity as previously discussed in the site-binding model.

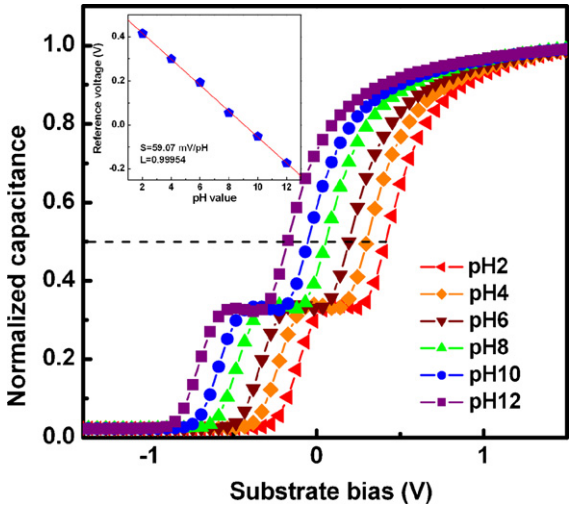

Fig. 3. *C–V* curves response of PrY_xO_y sensing films after PDA at 800 °C when inserted into solutions with pH values from 2 to 12. The inset shows reference voltage of a PrY_xO_y sensing film annealed at 800 °C as a function of pH at room temperature.

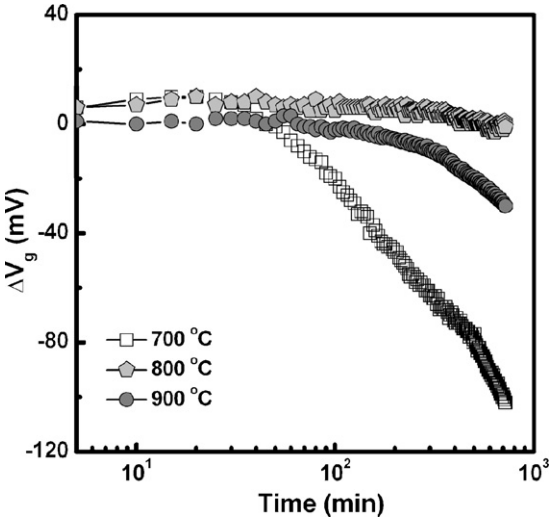

Fig. 5. Drift rate of EIS capacitors with PrY_xO_y sensing membranes annealed at different temperatures as a function of times in the pH=7 solution.

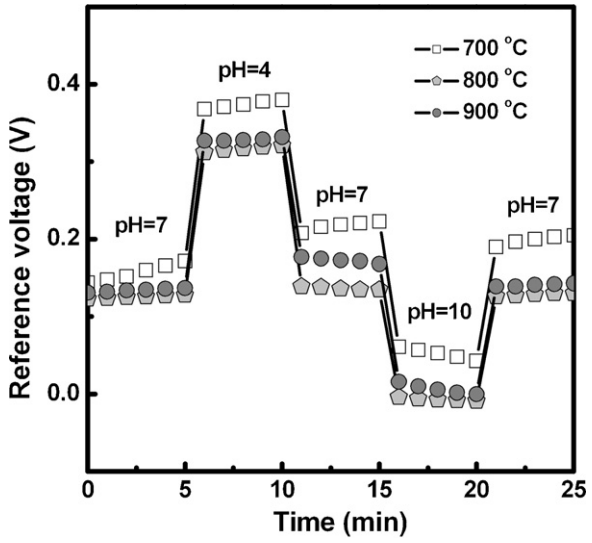

Fig. 4. Evaluation of hysteresis phenomenon of PrY_xO_y sensing films annealed at different temperatures in pH loop of 7 → 4 → 7 → 10 → 7.

Hysteresis phenomenon can be due to the defects of an insulator film, causing the formation of porous structures [23]. The interior sites of these porous detects could react with the ions existing in the tested solution and thus results in hysteresis response. Another possible cause is the interaction of ions in the tested solution with the responding sites along the boundaries of grains on an insulator film. We subjected the EIS capacitors prepared under the PrY_xO_y sensing film to pH loop of 7 → 4 → 7 → 10 → 7 over a period of 1500 s. The hysteresis voltage here is defined as the gate voltage difference between the initial and terminal voltages measured in the above pH loop. Fig. 4 and Table 2 revealed the profiles and the obtained hysteresis voltages of such evaluation, respectively. Fig. 4 illustrates that the hysteresis voltage of the EIS device incorporating a PrY_xO_y sensing film performed at the PDA of 800 °C had hysteresis voltages of 2.4 mV in the pH loop of 7 → 4 → 7 → 10 → 7. In addition, a PrY_xO_y EIS device annealed at 700 °C exhibited a higher hysteresis voltage than those of the devices prepared at the other RTA temperatures, as listed in Table 2. This could be due to a large number of crystal defects in the PrY_xO_y.

The drift rate of pH-ISFET is described using a hopping and/or trap-limited transport mechanism, also known as dispersive transport [24,25], to evaluate the hydration rate of the insulator. The phenomena of dispersive transport can be found in a broad class of disordered materials. In an amorphous material, for example, dispersive transport may result from hopping motion through localized states (hopping transport), trap-limited transport in the presence of traps possessing an exponential energy distribution (multiple-trap transport), or a combination of the aforementioned transport mechanisms (trap-controlled hopping transport) [25]. Dispersive transport causes a decay in the density of sites/traps occupied by the species going through transport [26]. The hypothesis that hydration of the gate dielectric is controlled by a dispersive transport mechanism is sustained by the presence of buried surface sites and/or the presence of traps (specifically electrically active silicon dangling bonds). The variations in the chemical composition of the insulator surface gives rise to the change in number of surface site with time, thus causing a monotonic temporal increase in the threshold voltage. Fig. 5 depicts the drift characteristics of EIS devices incorporating PrY_xO_y sensing membranes annealed at various temperatures, measured in solutions of pH 7 for 12 h. The PrY_xO_y EIS capacitor performed at 800 °C exhibited the best long-term stability (slope: 0.62 mV h^{-1}); in contrast, the EIS diode after PDA at 700 °C featured a serious drift of 7.68 mV h^{-1}. The lower drift effect after annealing at 800 °C arose from the low density of crystal defects. We suspect that higher drift rates is due to a lower surface roughness and a larger number of crystal defects producing the presence of buried surface sites and/or traps.

Table 2
The surface roughness, sensitivity, hysteresis voltage, and drift rate of high-*k* PrY_xO_y sensing membranes annealed at different temperatures.

RTA temperature (°C)	Surface roughness (nm)	Sensitivity (mV pH^{-1})	Hysteresis voltage (mV)	Drift rate (mV h^{-1})
700	0.394	53.51	39.4	7.68
800	0.743	59.07	2.4	0.62
900	0.649	56.69	6	2.57

The selectivity is one of the most important characteristics of an ion sensor, as it often determines whether a reliable measurement in the target sample is possible. Virtually all selectivity considerations based on the Nikolsky–Eisenman equation describe the potentiometric selectivity coefficients, $K^{pot}_{A,B}$ is the potentiometric selectivity coefficient for the primary ion A against the interfering ion B. According to the empirical Nikolsky–Eisenman Eq. (4) as follows:

$$E = E_0 + \frac{RT}{z_A F} \ln\left(a_A + \sum K^{pot}_{A,B} a_B^{Z_A/Z_B}\right) \quad (4)$$

where E is the measured electromotive force (emf); E_0 the constant that includes the standard potential of the electrode, the reference electrode potential, and the junction potential; R the gas constant ($8.314\,J\,K^{-1}\,mol^{-1}$); T the absolute temperature in Kelvin; F the Faraday constant ($96{,}490\,C\,mol^{-1}$); a_A the activity of primary ion, A, and a_B the activity of interfering ion, B; z_A an integer with sign and magnitude corresponding to the charge on the primary ion, A; z_B is an integer with same sign as z_A and magnitude corresponding to the charge on interfering ion, B; and $K^{pot}_{A,B}$ the potentiometric selectivity coefficient for ion B with respect to the primary ion A.

The selectivity coefficients of potentiometric ion sensors can be determined using different methods [27]. We performed the selectivity coefficients of PrY_xO_y EIS sensors for interfering ion Na^+ and K^+ with respect to the primary ion H^+. Separate solution method is employed to estimate the $K^{pot}_{H^+,Na^+}$ and $K^{pot}_{H^+,K^+}$ selectivity coefficients. Fig. 6 shows the reference voltage of PrY_xO_y EIS devices annealed at 800 °C vs. various H^+, Na^+, and K^+ ion concentration. The response curves were measured in the range of H^+, Na^+, and K^+ ion concentration from 10^{-5} to 0.05 M. We obtained selectivity coefficients of PrY_xO_y EIS sensors for ion Na^+ and K^+ at −5.34 and −5.17, respectively. It is evident that the EIS device incorporating a high-k PrY_xO_y sensing membrane was more responsive to H^+ relative to Na^+ and K^+.

The measured as well as extracted sensing parameters are summarized in Table 3, where the data from EIS devices fabricated a Si_3N_4 [28,29], Al_2O_3 [28,29], Ta_2O_5 [30], WO_3 [31], HfO_2 [32], Y_2O_3 [10], Pr_2O_3 [11], and $PrTiO_3$ [11] film, are shown for comparison. Although a PrY_xO_y sensing membrane has a slightly higher hysteresis and drift, the nitrogen incorporated into PrY_xO_y film can reduce the low-k silica layer at the PrY_xO_y/Si interface and hence improve the sensing characteristics [33].

Table 3
Comparison of sensing parameters for EIS device fabricated with a Si_3N_4, Al_2O_3, Ta_2O_5, WO_3, HfO_2, Y_2O_3, Pr_2O_3, $PrTiO_3$, and PrY_xO_y.

Sensing membrane	pH sensivity ($mV\,pH^{-1}$)	Hysteresis voltage (mV)	Drift rate ($mV\,h^{-1}$)
Si_3N_4	53–55	3	0.8
Al_2O_3	54–56	0.8	0.3
Ta_2O_5	55–58	<1	0.2
WO_3	45–56	15.7	7.2–26
HfO_2	45–58	5–30	2.5–125
Y_2O_3	56.09	13.6	1.24
Pr_2O_3	52.9	17.5	2.15
$PrTiO_3$	56.8	2.84	1.77
PrY_xO_y	59.07	2.4	0.62

3.3. Urea biosensor

The application of enzyme molecules as the recognition agent in pH–EIS-based sensing systems results in the development of highly selective biosensors. The sensor is virtually configured by combining pH-ISFET mechanism with an enzyme-immobilized film as aforementioned. The principle of sensing is based on the detection of pH alteration caused by the specific enzyme–substrate reaction. Urease catalyzes the hydrolysis of urea to ammonium, hydroxyl, and bicarbonate ions. The increase in the HO^- ion concentration generates a potential change at the electrode surface that is proportional to the urea concentration, in accordance with the reaction:

$$NH_2CONH_2 + 3H_2O \xrightarrow{urease} 2NH_4^+ + OH^- + HCO_3^-$$

In this work, a urea biosensor with a hybrid structure of urease-containing alginate film/PrY_xO_y membrane/p-Si EIS was constructed. Instead of enzyme immobilization by covalent bonding approach, entrapment method was adopted to immobilize the enzyme molecules onto PrY_xO_y sensing membrane in this case, providing a relatively milder condition to possibly minimize the loss of enzyme activity during immobilization process. In addition, the other feature of the design is that the prepared enzyme/alginate thin film is easy to prepare and is able to reversely attach on the surface of PrY_xO_y membrane. Particularly the latter potentially makes disposable urea biosensor possible by simply replacing the enzyme/hydrogel film when every time use. Fig. 7 presents the shift in the reference voltage of the enzymatic EIS-based urea biosensor

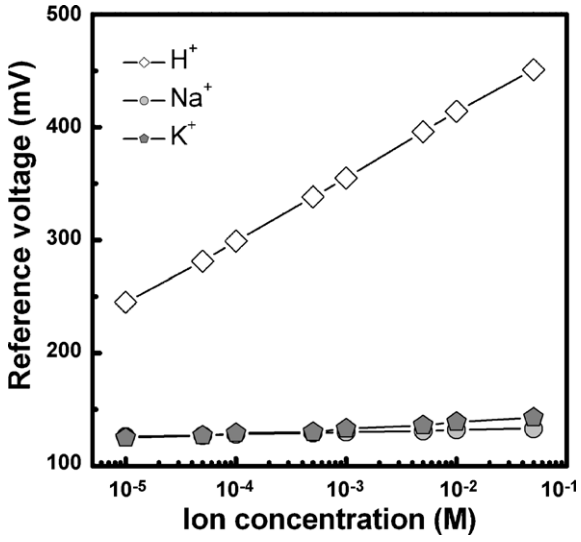

Fig. 6. Reference voltage of EIS devices incorporating PrY_xO_y sensing membranes annealed at 800 °C for different H^+, Na^+, and K^+ ion concentration in pH 7.16.

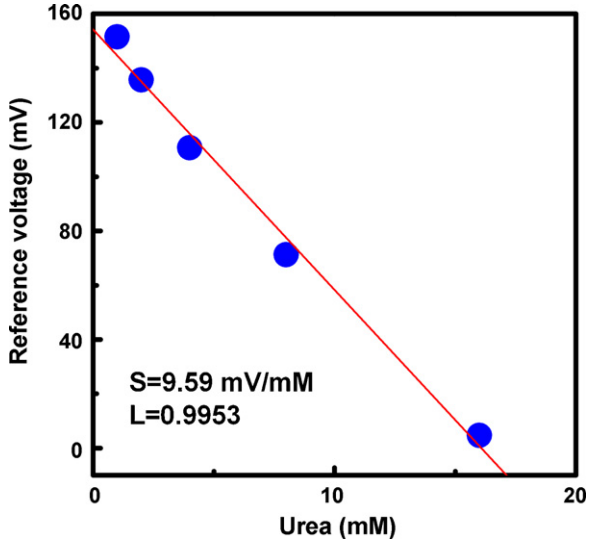

Fig. 7. The calibration curve of potentiometric urea biosensor based on a high-k PrY_xO_y EIS device.

incorporating a PrY_xO_y sensing film (RTA at 800 °C) as a function of the urea concentration. It is found that the presented device was able to detect urea with good linearity (R^2 = 0.99) and reasonable sensitivity of 9.59 mV mM^{-1} in the urea concentration range of 1 to 16 mM, which is sufficient for general clinical examination of blood urea.

4. Conclusions

In this study, we proposed high-performance EIS devices incorporating high-*k* PrY_xO_y sensing membranes grown on Si substrates by reactive co-sputtering. We used SIMS and AFM to confirm the presence of the PrY_xO_y structures in these EIS devices. The high-*k* PrY_xO_y EIS device that had been subjected to RTA at 800 °C exhibited an optimum pH sensing performance including a high sensitivity of 59.07 mV pH^{-1}, a small hysteresis voltage of 2.4 mV and a low drift rate of 0.62 mV h^{-1}. The selectivity coefficients of PrY_xO_y sensors for ion Na^+ and K^+ are at −5.34 and −5.17, respectively. This improvement is attributed to the lower number of crystal defects and the higher surface roughness occurred at this condition. Furthermore, an enzymatic EIS-based urea biosensor incorporating a PrY_xO_y sensing membrane exhibited a sensitivity towards the detection of urea of 9.59 mV mM^{-1}.

Acknowledgment

This work was supported by the National Science Council, Taiwan, Republic of China, under contract no. NSC-97-2221-E-182-050-MY3.

References

[1] P. Bergveld, IEEE Trans. Biomed. Eng. 17 (1970) 70.
[2] A. Fog, R. Buck, Sens. Actuators 5 (1984) 137.
[3] S. Caras, J. Janata, Anal. Chem. 52 (1980) 1935.
[4] L. Bousse, S. Mostarshed, B. van der Schoot, N.F. de Rooij, Sens. Actuators B 17 (1994) 157.
[5] S. Jamasb, S.D. Collins, R.L. Smith, IEEE Trans. Electron. Devices 45 (1998) 1239.
[6] H.K. Liao, J.C. Chou, W.Y. Chung, T.P. Sun, S.K. Hsiung, Sens. Actuators B 50 (1998) 104.
[7] J.C. Van Kerkhof, W. Olthuis, P. Bergveld, Sens. Actuators B 3 (1991) 129.
[8] D. Sobczynska, W. Torbicz, Sens. Actuators 6 (1984) 93.
[9] C.M. Yang, C.S. Lai, T.F. Lu, T.C. Wang, D.G. Pijanowska, J. Electrochem. Soc. 155 (2008) J326.
[10] T.M. Pan, K.M. Liao, Sens. Actuators B 127 (2007) 480.
[11] T.M. Pan, K.M. Liao, Sens. Actuators B 133 (2008) 97.
[12] L.B. Chang, H.H. Ko, Y.L. Lee, C.S. Lai, C.Y. Wang, J. Electrochem. Soc. 153 (2006) G330.
[13] Y.S. Lin, R. Puthenkovilakam, J.P. Chang, Appl. Phys. Lett. 81 (2002) 2041.
[14] T.M. Pan, F.J. Tsai, C.I. Hsieh, T.W. Wu, Electrochem. Solid-State Lett. 10 (2007) G21.
[15] H. Yamada, T. Shmizu, A. Kurokawa, K. Ishii, E. Suzuki, J. Electrochem. Soc. 150 (2003) G429.
[16] Y. Zhao, M. Toyama, K. Kita, K. Kyuno, A. Toriumi, Appl. Phys. Lett. 88 (2006) 072904.
[17] Y. Zhao, K. Kita, K. Kyuno, A. Toriumi, Appl. Phys. Lett. 89 (2006) 252905.
[18] L. Miotti, K.P. Bastos, C. Driemeier, V. Edon, M.C. Hugon, B. Agius, I.J.R. Baumvol, Appl. Phys. Lett. 87 (2005) 022901.
[19] C.D. Fung, P.W. Cheung, W.H. Ko, IEEE Trans. Electron. Devices 33 (1986) 8.
[20] L. Bousse, N.F. de Rooij, P. Bergveld, IEEE Trans. Electron. Devices 30 (1983) 1263.
[21] R.E.G. van Hal, J.C.T. Eijkel, P. Bergveld, Sens. Actuators B 24 (1995) 201.
[22] W. Torbicz, Z. Sypniewska, Sens. Actuators B 7 (1992) 565.
[23] L. Bousse, H.H. van den Vlekkert, N.F. de Rooij, Sens. Actuators B 2 (1990) 103.
[24] H. Scher, E.W. Montroll, Phys. Rev. B 12 (1975) 2455.
[25] G. Pfister, H. Scher, Phys. Rev. B 15 (1977) 2062.
[26] J. Kakalios, R.A. Street, W.B. Jackson, Phys. Rev. Lett. 59 (1987) 1037.
[27] E. Bakker, E. Pretsch, P. Bhlmann, W.B. Jackson, Anal. Chem. 72 (2000) 1127.
[28] Y. Miao, J. Guan, J. Chen, Biotechnol. Adv. 21 (2003) 527.
[29] T. Matsuo, M. Esashi, H. Abe, IEEE Trans. Electron. Devices 26 (1979) 1856.
[30] A. Poghossian, M.J. Schoning, Electroanalysis 16 (2004) 1863.
[31] J.L. Chiang, S.S. Jan, J.C. Chou, Y.C. Chen, Sens. Actuators B 76 (2001) 624.
[32] C.S. Lai, C.M. Yang, T.F. Lu, Electrochem. Solid-State Lett. 9 (2006) G90.
[33] P.D. Kirsch, C.S. Kang, J. Lozano, J.C. Lee, J.G. Ekerdt, J. Appl. Phys. 91 (2002) 4353.